ChemPubSoc Europe

DOI: 10.1002/celc.201500016

CHEMELECTROCHEM Articles

Ferrocene-Boronic Acid–Fructose Binding Based on Dual-Plate Generator–Collector Voltammetry and Square-Wave Voltammetry

Meng Li,[a] Su-Ying Xu,[a] Andrew J. Gross,[a] Jules L. Hammond,[b] Pedro Estrela,[b] James Weber,[a] Karel Lacina,[c] Tony D. James,[a] and Frank Marken*[a]

The interaction of ferrocene-boronic acid with fructose is investigated in aqueous 0.1 M phosphate buffer at pH 7, 8 and 9. Two voltammetric methods, based on 1) a dual-plate generator–collector micro-trench electrode (steady state) and 2) a square-wave voltammetry (transient) method, are applied and compared in terms of mechanistic resolution. A combination of experimental data is employed to obtain new insights into the binding rates and the cumulative binding constants for both the reduced ferrocene-boronic acid (pH dependent and weakly binding) and for the oxidised ferrocene-boronic acid (pH independent and strongly binding).

1. Introduction

Boronic acids have emerged as key components in analytical processes and devices,[1] for example, for the detection and monitoring of glucose levels[2] and for the separation of glycated and glycosylated proteins,[3] both of which are applications with considerable potential in medicinal technologies. Chemically, boronic acids are attractive, owing to their capability to reversibly form bonds to diols,[4] quinols,[5] α-hydroxy-carboxylates[6] and a range of other hard nucleophiles, in particular fluoride[7] and phosphate.[8] New types of boronic acids have been developed to report binding events through fluorescence[9] or electrochemical responses[10] for operation in more opaque or non-transparent media. The ferrocene-boronic acid compound (see Scheme 1) may be regarded as a prototypical electrochemical reporter system.[11,12,13]

Most electrochemically active boronic-acid systems have a structurally defined redox moiety and a separate boronic-receptor moiety without a strong interaction between the two. As a result, the electrochemical signal is not strongly affected by binding (only the diffusion coefficient changes; no significant changes in the midpoint potential are observed). However, in ferrocene-boronic acid a stronger coupling occurs, with the Fe(II/III) redox state directly affecting the binding kinetics and binding energies. The classic square-scheme mechanism in Scheme 1 can be applied (although further complexity, owing to intermediates and ternary complexes, for example, with phosphate,[14] clearly exists).

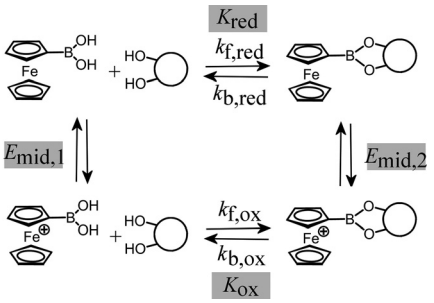

Scheme 1. Representation of the square-scheme mechanism[15] for the binding of fructose to ferrocene-boronic acid in two different redox states.

The fact that the ferrocene-boronic acid redox signal can be directly employed to report on fructose (or other saccharides) binding is of interest and the conditions required for two distinct signals to be detected are important. Therefore, in this study, the binding process is investigated with two voltammetric methods: a steady-state method (dual-plate generator–collector voltammetry)[16,17] and a method that is transient in nature (square-wave voltammetry).[18] The ability of these two experimental tools to distinguish and quantify bound and unbound ferrocene-boronic acid are compared.

When detecting two distinct voltammetric signals associated with unbound and bound configurations, it may be tempting to interpret these signals in terms of equilibrium concentrations and binding constants (K_{red}, K_{ox}). However, within the limit of fast experimental tools, it is more likely that the rate of binding is responsible for the splitting and magnitude of the voltammetric responses ($k_{f,ox}$, $k_{f,red}$). To dissect and determine the true binding constants (as a function of pH), a deeper analysis of the data is required. In (simplified) Scheme 1, there are

[a] M. Li, Dr. S.-Y. Xu, Dr. A. J. Gross, J. Weber, Prof. T. D. James, Prof. F. Marken
Department of Chemistry
University of Bath, Claverton Down, Bath BA2 7AY (UK)
E-mail: f.marken@bath.ac.uk

[b] J. L. Hammond, Dr. P. Estrela
Department of Electronic and Electrical Engineering
University of Bath, Claverton Down, Bath BA2 7AY (UK)

[c] Dr. K. Lacina
CEITEC, Masaryk University
Kamenice 5, CS-62500 Brno (Czech Republic)

five unknown parameters (two midpoint potentials and four rate constants, minus one thermodynamic relationship linking these, vide infra), all of which are shown to be relevant. Data have been analysed for pH 7, 8 and 9 to demonstrate distinct trends in the interaction of fructose with ferrocene- and ferricenium-boronic acids.

Experimental Section

Chemical Reagents

Potassium chloride (≥99%) and hydrogen peroxide (30 wt% in water) were purchased from Sigma–Aldrich, UK. Hexaammineruthenium (III) chloride [$Ru(NH_3)_6Cl_3$, 99%] and SU8-2002 negative photoresist were purchased from Strem Chemicals and Microchem Corp., respectively. Ferrocene-boronic acid (>98%) was purchased from Tokyo Chemical Industry Co., Ltd, sodium dihydrogen phosphate was used as a buffer salt, as purchased from Fisher Scientific, and fructose (99%) was purchased from Alfa Aesar. Demineralised and filtered water was taken from a Vivendi water purification system with no less than 18 MΩ cm resistivity.

Instrumentation

Square-wave voltammetry was performed on a microAutolab III system (Metrohm-Autolab, Netherlands) in staircase-voltammetry mode. The step potential was maintained at approximately 1 mV. The counter and reference electrodes were platinum gauze and saturated calomel (SCE, Radiometer), respectively. The working electrode was a 2.0 mm-diameter platinum-disc electrode. Rotating-disc voltammetry was performed with a Gamry 710 system. Solutions were de-aerated with argon (BOC). All experiments were conducted at 22±2 °C.

Electrochemical dual-plate generator–collector experiments were performed on a SP-300 bipotentiostat (Biologic, France). A four-electrode cell was employed with a Pt-wire counter electrode, a SCE (Radiometer), and the working electrodes of the micro-trench electrode. A PWM32 spin coater was used to spin photoresist. Platinum films on glass substrates were prepared through electron-beam evaporation.

Fabrication and Calibration of Pt–Pt Dual-Plate Electrodes

Pt–Pt dual-plate micro-trench electrodes were fabricated following a previously reported protocol.[19] Glass slides were plasma treated (Oxford Instruments PlasmaPro 100) prior to deposition to improve adhesion. By using an electron-beam evaporator (Edwards FL-400), a 50 nm Ti adhesion layer, followed immediately by a 150 nm Pt (99.99% purity; Testbourne) layer, was deposited at 10^{-6} Torr through a custom-made stainless-steel shadow mask (Tecan). Film thicknesses were confirmed by using a mechanical contact profilometer (Dektak 6 M). The glass slide was subsequently cut into 8× 25 mm^{-2} Pt substrates by using a diamond cutter (Buehler, Isomet 1000 precision saw), which were then cleaned by rinsing with demineralised water and heat treatment at 450 °C. The dual-plate electrode was prepared by spin-coating a single layer of SU-8-2002 photoresist (MicroChem) onto two individual Pt substrates at 500 rpm for 15 s, then at 3000 rpm for 30 s. Next, the two electrodes were pushed together, face-to-face, and then placed on a hot plate at 90 °C for 2 min. The temperature was subsequently ramped to 160 °C and held for a further 5 min. After cooling to room temperature, the end of the dual-plate electrode was sliced by using the diamond cutter. The electrode was then immersed in Piranha solution (1:5 v/v H_2O_2/H_2SO_4; *Warning: Piranha solution is highly corrosive and appropriate precautions are needed*) for 30 min to etch the photoresist, giving a micro-trench with a width of 2.5 mm and an inter-electrode gap of $\delta = 5$ μm (see Figure 1). After etching, the electrode was rinsed with demineralised water then dried with a stream of nitrogen gas; copper tape was applied to provide two electrode contacts.

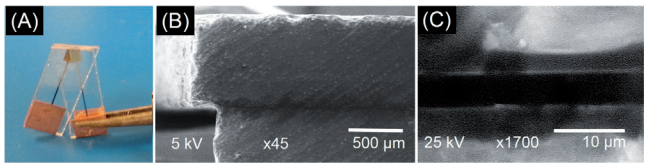

Figure 1. A) Photograph of the Pt–Pt dual-plate micro-trench electrode. B,C) Scanning electron microscopy images of the 2.5 mm long and 5 μm wide inter-electrode gap.

To estimate the depth of the Pt–Pt dual-plate electrode system, calibration voltammetric responses were recorded by using the $Ru(NH_3)_6^{3+/2+}$ redox system (1 mM) in aqueous 0.1 M KCl (Figure 2B). From the mass-transport-controlled limiting current obtained, 0.7 μA, and assuming equal diffusion coefficients for $Ru(NH_3)_6^{3+}$ and $Ru(NH_3)_6^{2+}$ ($D = 0.9\times10^{-9}$ $m^2 s^{-1}$),[20] the approximate depth was obtained as 16 μm[21] [see Eq. (1)]:

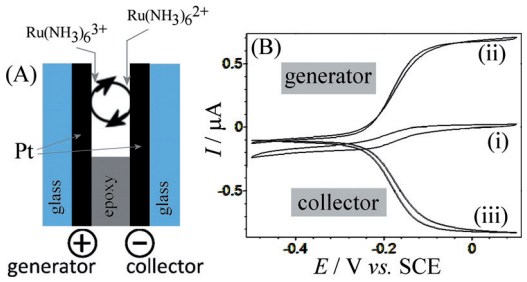

Figure 2. A) Schematic drawing of the Ru(II/III) redox couple in the Pt–Pt dual-plate generator–collector experiment. B) Cyclic voltammograms (scan rate 20 $mV s^{-1}$) for the reduction of 1 mM $Ru(NH_3)_6^{3+}$ in aqueous 0.1 M KCl with only one electrode connected (i) and with both generator and collector working electrodes connected (ii, iii); collector potential = −0.5 V vs. SCE.

$$\text{depth} = \frac{I_{lim} \times \delta}{nFDc \times \text{length}} = 16\ \mu\text{m} \qquad (1)$$

in which I_{lim} is the limiting current, δ is the inter-electrode gap, n is the number of electrons transferred for each molecule diffusing to the electrode surface, F is the Faraday constant, D is the diffusion coefficient, c is the bulk concentration and length/depth refer to the micro-trench length and depth.

2. Results and Discussion

2.1. Steady-State Dual-Plate Generator–Collector Micro-Trench Voltammetry

The oxidation of ferrocene-boronic acid in 0.1 M phosphate buffer (pH 7) occurs with a midpoint potential ($E_{mid} = {}^1/_2 E_{ox} + {}^1/_2 E_{red}$) of 0.14 V versus SCE (see Table 1) and is seen as an oxi-

Table 1. Summary of voltammetric equilibrium potential and kinetic data for the binding of fructose to ferrocene-boronic acid and ferricenium-boronic acid in 0.1 M phosphate buffer.

pH	$E_{mid,1}$ [V vs. SCE]	$E_{mid,2}$ [V vs. SCE]	$k_{f,ox}$ [$M^{-1}s^{-1}$]	K_{ox} [M^{-1}]	$k_{f,red}$ [$M^{-1}s^{-1}$]	K_{red} [M^{-1}]
7	+0.14	−0.04	120	300	12	0.27
8	+0.09	−0.04	240	400	24	2.5
9	+0.04	−0.03	670	300	67	20

dation at the generator electrode and a corresponding reduction at the collector electrode (see Figure 3A). Owing to the collector potential being fixed at −0.3 V versus SCE, the collector current signal is better defined and employed here for further analysis. Upon the addition of fructose, a new and more negative voltammetric signal emerges at $E_{mid} = -0.04$ V versus SCE, and this can be attributed to a boronic acid–fructose complex ($E_{mid,2} < E_{mid,1}$).[22,23] When formulating the equilibrium equations,[24] this is consistent with oxidised ferricenium-boronic acid, forming a stronger complex [$K_{ox} > K_{red}$; see Eq. (2)]:

$$RT \ln\left(\frac{K_{ox}}{K_{red}}\right) = -nF\left(E_{mid,2} - E_{mid,1}\right) \quad (2)$$

On the molecular scale, this may be attributed to more electropositive boron, but also changes in ion-association energies (e.g. involving phosphate anion–ferricenium cation interactions) could contribute to this effect. The mass-transport-controlled limiting current in the absence of fructose is close to 0.5 μA, which translates to an approximate diffusion coefficient of 0.6×10^{-9} $m^2 s^{-1}$ [Eq. (3)].[25,26] This value is not unreasonable for the free ferrocene-boronic acid and has been verified by independent rotating-disc voltammetry measurements [$D = 0.56 \times 10^{-9}$ $m^2 s^{-1}$ in 0.1 M phosphate buffer (pH 7)]:

$$D = \frac{I_{lim} \times \delta}{nFc \times \text{depth} \times \text{length}} = 0.6 \times 10^{-9}\ m^2\ S^{-1} \quad (3)$$

With increasing fructose levels, the mass-transport-controlled limiting current decreases naturally, owing to underlying changes in solution viscosity. The plot in Figure 3A shows a gradual decrease in collector current followed by a stronger decline from a fructose concentration of 160 mM onwards. The more pronounced decline in mass-transport-limited current coincides with the appearance of the signal at $E_{mid,2}$ and is, therefore, assigned to binding of boronic acid to fructose. Similar data sets are presented for pH 8 and pH 9 in Figure 3B and Figure 3C, respectively.

To better describe the boronic acid–fructose binding process, kinetic domains are introduced (Figure 3D). In domain I, both ferrocene-boronic acid and ferricenium-boronic acid are "free" and the limiting current is relatively high. It is only in domain II that the ferricenium-boronic acid will bind to fructose, thereby lowering the rate of diffusion (the lower diffusion coefficient dominates the inter-electrode transport).[27] In domain III, the fructose concentration is so high that both ferrocene- and

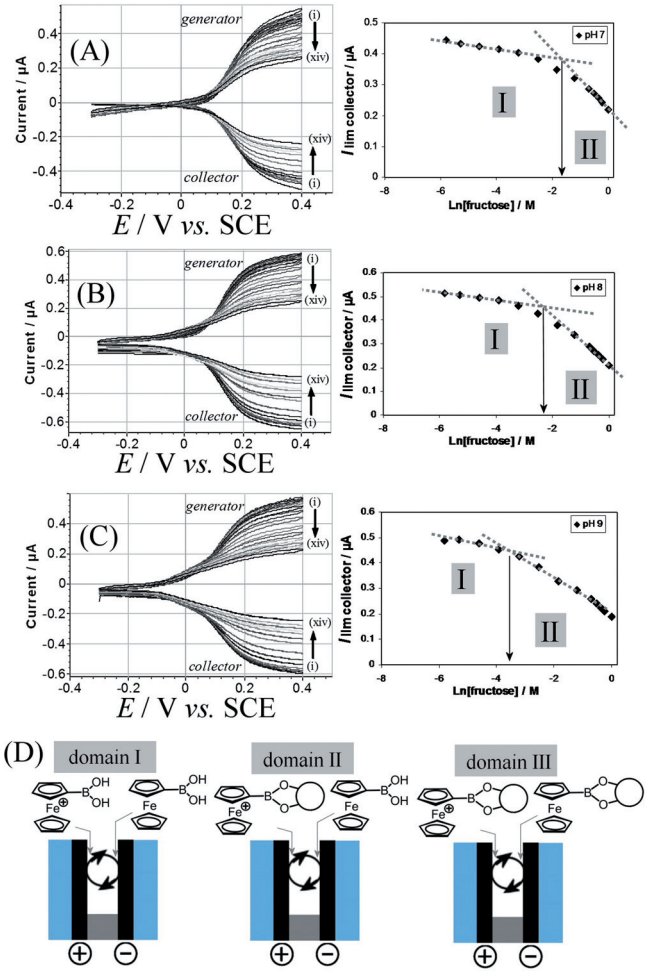

Figure 3. Dual-plate generator–collector voltammograms (scan rate 20 mV s^{-1}, collector potential −0.3 V vs. SCE) for the oxidation of 1 mM ferrocene-boronic acid in 0.1 M phosphate buffer with a fructose concentration of i) 1, ii) 3, iii) 5, iv) 10, v) 20, vi) 40, vii) 80, viii) 160, ix) 300, x) 500, xi) 600, xii) 700, xiii) 800 and xiv) 1000 mM at A) pH 7, B) pH 8 and C) pH 9; the corresponding plots of the collector limiting current versus the logarithm of fructose concentration are shown to the right-hand side. D) Schematic drawing of the redox cycle kinetic domains, showing domain I with no fructose bound, domain II with fructose binding to the ferricenium-boronic acid and domain III with fructose binding to both ferrocene- and ferricenium-boronic acids.

ferricenium-boronic acids bind (with little further change in the transport). The transition point from domain I to II (see Figure 3) is consistent with the reaction layer, which is approximately given by Equation (4)[28] and is equal to the inter-electrode gap of 5 μm.

$$\delta_{reaction} = \sqrt{\frac{D}{k_f[\text{fructose}]}} \quad (4)$$

Approximate rate constant data for $k_{f,ox}$ can be obtained (see Table 1) and a clear trend of an increasing $k_{f,ox}$ value with increasing pH is observed. At a molecular level, this can be interpreted, for example, in terms of a fast pre-equilibrium involving hydroxide or HPO_4^{2-}.

Owing to dual-plate generator–collector voltammetry offering a very fast steady-state measurement tool, only kinetic information is obtained and additional information from a transient measurement method, for example from square-wave voltammetry, is needed for the evaluation of the associated binding constants.

2.2. Transient Macro-Disc Square-Wave Voltammetry

Square-wave voltammetry is commonly employed as an analytical tool for binding and analytical assays.[29] Here, the oxidation of ferrocene-boronic acid is studied at a 2 mm diameter platinum electrode immersed in 0.1 M phosphate buffer solution at pH 7, 8 and 9. Figure 4A shows a typical data set, whereby addition of fructose causes an initial peak at 0.14 V versus SCE to shift and then split to give a new peak at −0.04 V versus SCE. These two peaks are associated with $E_{mid,1}$ and $E_{mid,2}$ for the oxidation of ferrocene-boronic acid without and with fructose attached, respectively.

Similar to the case of data from dual-plate generator–collector voltammetry, it is likely that the rate constant $k_{f,ox}$ is dominating the shape of this voltammetric signal with the frequency of $f = 8.3$ Hz being linked to a typical diffusion layer of $\delta_{diffusion} = \sqrt{D/f} = 8\mu m$. When the peak-current data are plotted against the logarithm of fructose concentration, a crossing point is observed at 370 mM (Figure 4A), which is not too dissimilar to the transition point in the steady-state voltammetric response (Figure 3A). Therefore, the values for $k_{f,ox}$ evaluated above were employed as a starting point for the analysis.

When digital simulation is employed, $E_{mid,1}$, $E_{mid,2}$ and $k_{f,ox}$ can be used as known input parameters. When first looking at the crossing point with 370 mM fructose, the peak ratio is consistent with $K_{ox} = 300\ M^{-1}$ (through trial-and-error simulation), whereas for the peak-to-peak separation to then be correct, $k_{f,red}$ requires to be approximately ten times slower than $k_{f,ox}$. This completes the set of five required parameters to solve the square scheme in Scheme 1, at least as a first approximation. A full optimisation of this solution with sensitivity analysis for each parameter with error evaluation would be desirable, but is currently not possible. A full set of simulated square-wave voltammetric curves for pH 7 is shown in Figure 4A. There are some remaining approximations in the input parameters (the diffusion coefficients are fixed at $D = 0.5\times10^{-9}\ m^2 s^{-1}$ for all species and electron transfer is assumed reversible) and, therefore, the resulting equilibrium and rate constants need to be considered as estimates. However, the relatively good agreement between the shape of the simulated signals and the experimental data is reassuring (simulated peak currents at high fructose levels appear slightly higher, owing to the missing effect of lower diffusion rates). A plot of the peak currents from the simulation data versus a logarithm of fructose concentration (see Figure 4A plot lines) confirms the agreement. Similarly, data analysis was performed for pH 8 and pH 9, and the parameters are summarised in Table 1.

The effect of the square-wave frequency on the voltammetric signal (for pH 8 with 80 mM fructose) is demonstrated in Figure 4D, where only a slight increase in the peak-to-peak separation with frequency is observed, thus confirming the analysis method chosen above. At higher frequency, a broad background response also emerges, which is possibly associated with the adsorbed species. The trend in binding constants with pH is shown in Figure 4E. Perhaps surprisingly, the binding constant K_{ox} for the ferricenium-boronic acid is not significantly affected by the pH value and only the weaker K_{red} for the ferrocene-boronic acid strengthens with increasing pH. The observed trends could be linked to the formation of ternary complexes involving hydroxide or phosphate.

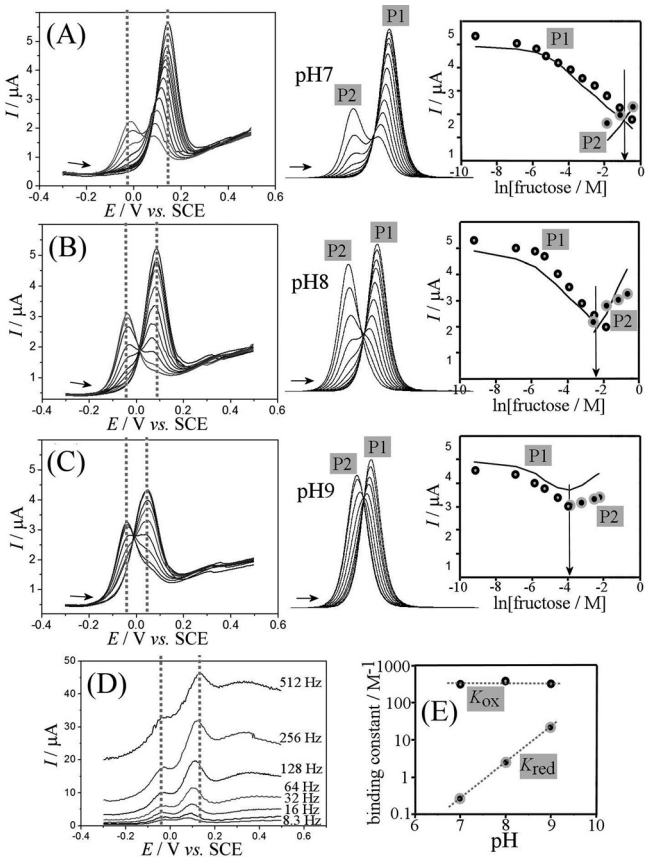

Figure 4. Square-wave voltammograms ($f = 8.3$ Hz, from −0.3 to +0.5 V vs. SCE, potential step 5 mV, amplitude 10 mV, 2 mm-diameter platinum disc) for the oxidation of 1 mM ferrocene-boronic acid in A) 0.1 M phosphate buffer (pH 7) with 0, 1, 3, 5, 10, 20, 40, 80, 160, 320 and 640 mM fructose, B) 0.1 M phosphate buffer (pH 8) with 0, 1, 3, 5, 10, 20, 40, 80, 160, 300, and 500 mM fructose and C) 0.1 M phosphate buffer (pH 9) with 0, 1, 3, 5, 10, 20, 40, 80, and 100 mM fructose. Also shown are the DigiElch simulations and the plot of peak currents for experimental (symbols) and simulation (line) data based on $D = 0.5\times10^{-9}\ m^2 s^{-1}$ for all species. D) Square-wave voltammograms at pH 8 for 80 mM fructose as a function of frequency. E) Plot of the binding constants K_{ox} and K_{red} versus pH.

3. Conclusions

Voltammetric data for the interaction of ferrocene-boronic acid with fructose (or other saccharides) are time-domain sensitive and here demonstrated for 1) a fast steady-state method based on dual-plate generator–collector voltammetry and 2) a fast transient method based on square-wave voltammetry. Information from voltammetric peaks for bound and unbound

forms of the ferrocene-boronic acid are predominantly attributed to the kinetic parameter $k_{f,ox}$ for the rate of binding to the oxidised ferricenium-boronic acid. To extract additional information (in particular binding constants), numerical simulation tools are required and data sets for a range of fructose concentrations need to be compared. A more detailed analysis of the data could take into account additional parameters for changes in diffusion coefficients with viscosity and changes in the rate of electron transfer. It is interesting to note that these results suggest kinetic resolution as an analytical approach, where the boronic-acid receptor is employed to detect fast-binding analytes at higher sensitivities compared to slow-binding analytes. A further conclusion emerging from this study is the possibility to develop a switchable boronic acid,[30] for example, to be used in separation processes at suitably adjusted pH values.

Acknowledgements

J.L.H. is supported by a UK Engineering and Physical Sciences Research Council (EPSRC) Doctoral Training Award. A.J.G. and F.M. gratefully acknowledge EPSRC funding (EP/I028706/1). K.L. acknowledges support from the CEITEC facility (CZ.1.05/1.1.00/02.0068). T.D.J. and M.L. are grateful for financial support from China Scholarship Council (CSC) and from University of Bath Full Fees Scholarship.

Keywords: boronic acids · electroanalysis · ferrocene · saccharides · voltammetry

[1] T. D. James, M. D. Phillips, S. Shinkai, *Boronic acids in saccharide recognition*, RSC, Cambridge, **2006**.
[2] S. D. Bull, M. G. Davidson, J. M. H. Van den Elsen, J. S. Fossey, A. T. A. Jenkins, Y. B. Jiang, Y. Kubo, F. Marken, K. Sakurai, J. Z. Zhao, T. D. James, *Acc. Chem. Res.* **2013**, *46*, 312 – 326.
[3] J. S. Fossey, F. D'Hooge, J. M. H. van den Elsen, M. P. P. Morais, S. I. Pascu, S. D. Bull, F. Marken, A. T. A. Jenkins, Y. B. Jiang, T. D. James, *Chem. Rec.* **2012**, *12*, 464 – 478.
[4] J. P. Lorand, J. O. Edwards, *J. Org. Chem.* **1959**, *24*, 769 – 774.
[5] K. Lawrence, T. Nishimura, P. Haffenden, J. M. Mitchels, K. Sakurai, J. S. Fossey, S. D. Bull, T. D. James, F. Marken, *New J. Chem.* **2013**, *37*, 1883 – 1888.
[6] N. Katif, R. A. Harries, A. M. Kelly, J. S. Fossey, T. D. James, F. Marken, *J. Solid State Electrochem.* **2009**, *13*, 1475 – 1482.
[7] X. Wu, X. X. Chen, B. N. Song, Y. J. Huang, W. J. Ouyang, Z. Li, T. D. James, Y. B. Jiang, *Chem. Commun.* **2014**, *50*, 13987 – 13989.
[8] M. Li, G. E. M. Lewis, T. D. James, Y. T. Long, B. Kasprzyk-Hordern, J. M. Mitchels, F. Marken, *ChemElectroChem* **2014**, *1*, 1640 – 1646.
[9] Y. J. Huang, W. J. Ouyang, X. Wu, Z. Li, J. S. Fossey, T. D. James, Y. B. Jiang, *J. Am. Chem. Soc.* **2013**, *135*, 1700 – 1703.
[10] J. S. Hansen, J. B. Christensen, J. F. Petersen, T. Hoeg-Jensen, J. C. Norrild, *Sens. Actuators B* **2012**, *161*, 45 – 79.
[11] C. Dusemund, K. R. A. S. Sandanayake, S. Shinkai, *J. Chem. Soc. Chem. Commun.* **1995**, 333 – 334.
[12] A. Q. Liu, U. Wollenberger, M. Katterle, F. W. Scheller, *Sens. Actuators B* **2006**, *113*, 623 – 629.
[13] K. Lacina, P. Skladal, *Electrochim. Acta* **2011**, *56*, 10246 – 10252.
[14] L. I. Bosch, T. M. Fyles, T. D. James, *Tetrahedron* **2004**, *60*, 11175 – 11190.
[15] A. M. Bond, S. W. Feldberg, H. B. Greenhill, P. J. Mahon, R. Colton, T. Whyte, *Anal. Chem.* **1992**, *64*, 1014 – 1021.
[16] S. E. C. Dale, F. Marken in *SPR Electrochemistry, Vol. 12*, (Eds.: R. G. Compton, J. D. Wadhawan), RSC, Cambridge, **2013**, pp. 132 – 154.
[17] S. E. C. Dale, C. E. Hotchen, F. Marken, *Electrochim. Acta* **2013**, *101*, 196 – 200.
[18] V. Mirceski, R. Gulaboski, *Maced. J. Chem. Chem. Eng.* **2014**, *33*, 1 – 12.
[19] A. J. Gross, F. Marken, *Electrochem. Commun.* **2014**, *46*, 120 – 123.
[20] F. Marken, J. C. Eklund, R. G. Compton, *J. Electroanal. Chem.* **1995**, *395*, 335 – 339.
[21] A. J. Gross, S. Holmes, S. E. C. Dale, M. J. Smallwood, S. J. Green, C. P. Winlove, N. Benjamin, P. G. Winyard, F. Marken, *Talanta* **2015**, *131*, 228 – 235.
[22] K. Lacina, J. Novotny, Z. Moravec, P. Skladal, *Electrochim. Acta* **2015**, *153*, 280 – 286.
[23] J. W. Tomsho, S. J. Benkovic, *J. Org. Chem.* **2012**, *77*, 2098 – 2106.
[24] S. X. Guo, S. W. Feldberg, A. M. Bond, D. L. Callahan, P. J. S. Richardt, A. G. Wedd, *J. Phys. Chem. B* **2005**, *109*, 20641 – 20651.
[25] A. T. Hubbard, D. G. Peters, *Crit. Rev. Anal. Chem.* **1973**, *3*, 201 – 242.
[26] M. A. Hasnat, A. J. Gross, S. E. C. Dale, E. O. Barnes, R. G. Compton, F. Marken, *Analyst* **2014**, *139*, 569 – 575.
[27] S. E. C. Dale, A. Vuorema, M. Sillanpää, J. Weber, A. J. Wain, E. O. Barnes, R. G. Compton, F. Marken, *Electrochim. Acta* **2014**, *125*, 94 – 100.
[28] F. Marken, A. Neudeck, A. M. Bond in *Electroanalytical Methods*, (Ed.: F. Scholz), Springer, Berlin, **2010**, pp. 89 – 106.
[29] E. Laborda, J. Gonzalez, A. Molina, *Electrochem. Commun.* **2014**, *43*, 25 – 30.
[30] A. N. J. Moore, D. D. M. Wayner, *Can. J. Chem.* **1999**, *77*, 681 – 686.

Received: January 17, 2015
Published online on February 25, 2015

